ACS APPLIED MATERIALS & INTERFACES

www.acsami.org
Research Article

Squaraine-Peptide Conjugates as Efficient Reporters of Neutrophil Extracellular Traps-Mediated Chronic Inflammation

Sai Kiran Mavileti,*,# Galyna Bila,# Valentyn Utka, Rostyslav Bilyy, Jr., Evgenia Bila, Elena Butoi, Shekhar Gupta, Priyanka Balyan, Tamaki Kato, Rostyslav Bilyy,* and Shyam S. Pandey*

Cite This: ACS Appl. Mater. Interfaces 2025, 17, 9140−9154
Read Online

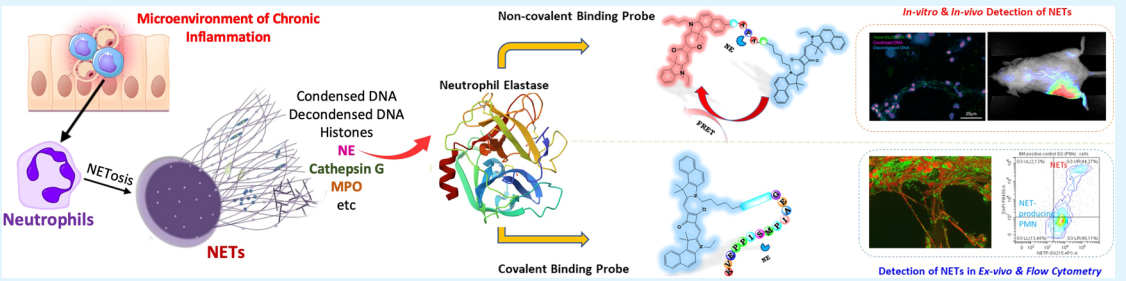

ABSTRACT: The excessive and uncontrolled release of neutrophil extracellular traps (NETs) is increasingly linked to the pathogenesis of various inflammatory diseases, cardiovascular disorders, and cancers. Real-time, non-invasive detection of NETs is crucial for understanding their role in disease progression and developing targeted therapies. Current NETs detection methods often lack the necessary specificity and resolution, particularly in vivo and ex vivo settings. To address this, we have developed novel near-infrared squaraine-peptide conjugates by rational molecular design as reporters of NETosis by targeting the protease activity of neutrophil elastase (NE). These self-quenching, cell-impermeable probes enable the precise real-time detection and imaging of NETs. The Förster resonance energy transfer (FRET)-based probe, **Hetero-APA**, demonstrated high specificity in detecting NETs in vitro and in vivo, generating strong fluorescence in NETs-rich environments. To overcome the limitations of FRET-based probes for ex vivo imaging, we designed **SQ-215-NETP**, a non-FRET-based probe that covalently binds to the NE. **SQ-215-NETP** achieved an unprecedented imaging resolution of 90 nm/pixel in human coronary thrombi, marking the first report of such high resolution with a low molecular weight probe. Additionally, **SQ-215-NETP** effectively detected NETs by flow cytometry. These results highlight the potential of these probes in NETosis detection, offering promising tools for enhanced diagnostics and therapeutic strategies in managing NET-mediated inflammatory diseases and cancers.

KEYWORDS: *chronic inflammation, near-infrared probes, NETosis, NETs detection & imaging, neutrophil elastase, squaraine-peptide conjugates*

1. INTRODUCTION

Neutrophils form the frontline of the innate immune system, which coordinates a complex defense response against invading pathogens and infections through phagocytosis, degranulation, and reactive oxygen species (ROS) production.[1,2] In the recent past, neutrophil extracellular traps (NETs) have come to great prominence as an entirely novel aspect of the defense mechanism of neutrophils. NETs are web-like structures released by activated neutrophils, composed of decondensed chromatin and antimicrobial proteins, to entrap and kill invading pathogens, such as bacteria, viruses, and fungi. NETs are characterized by condensed DNA, histones, neutrophil elastase (NE), cathepsin G, myeloperoxidase (MPO), etc. NE plays a crucial role in NET formation, cleaving histones and other proteins to facilitate chromatin decondensation.[3,4] NE, a serine protease, has broad substrate specificity that enables the degradation of bacterial components, facilitating phagocytosis, and clearance.[5,6] Furthermore, NE also cleaves extracellular matrix proteins such as elastin and collagen, promoting neutrophil migration and tissue remodeling during inflammation.[7−9] However, its uncontrolled and unregulated activity can inflict adverse effects, degrading host tissues and exacerbating inflammatory responses.[10] This destructive potential is evident in diseases like chronic obstructive pulmonary disease, pancreatitis,[11] inflammatory bowel disease,[12] atherosclerosis,[13] and acute lung injury (ALI), where uncontrolled NE contributes to tissue destruction and impaired lung function.[14−16]

Received: November 26, 2024
Revised: January 17, 2025
Accepted: January 24, 2025
Published: February 3, 2025

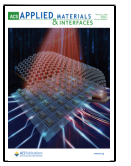

Despite their beneficial role in host defense, NETs are known to play pivotal roles in many inflammatory diseases and cancer.[17] Their unregulated and uncontrolled release can exacerbate inflammation and contribute to the development of autoimmune diseases and thrombosis.[18,19] Aberrant NETs formation has been linked to pulmonary diseases like acute respiratory distress syndrome, ALI,[20] and COVID-19,[21] where NE was shown to actively contribute to lung remodeling cleaving elastin and fostering fibrosis resulting in lung stiffness. NETs also induce the release of inflammatory cytokines, amplifying the inflammatory response and aggravating lung injury.[22,23] Chronic NETs release can also contribute to lung fibrosis, in other lung diseases.[24,25] NETs also contribute to tumor growth and metastasis significantly.[26−29] Therefore, unraveling the intricate interplay among NE, NETs, and pathogenesis promises significant advancements in our understanding of inflammatory pathogenesis and cancer development. This opens new avenues for the development of noninvasive diagnostic tools, more importantly targeting NETs and NE activity,[17] thereby leading to better therapeutic strategies and disease monitoring.

Activity-based fluorescent probes that exploit the protease activity of NE enable noninvasive, real-time detection of NETs in tumor and inflammatory environments. This capability allows for precise monitoring and visualization of NETs, thereby tracking disease progression accurately. Fluorescence emissions in the near-infrared (NIR) wavelength region are particularly significant because emissions in the visible range are often compromised by the autofluorescence of intrinsic biomolecules and proteins, which generate substantial background noise, severe light scattering, and a reduced signal-to-noise ratio, ultimately leading to poor imaging quality. In contrast, compounds that absorb and emit light in the NIR region provide higher sensitivity, deeper tissue penetration, lower light scattering, and a very high signal-to-noise ratio due to the minimal natural autofluorescence of biomolecules.[30−33] Despite some reports on NIR imaging of NE,[34−36] only a limited number of probes have been specifically designed to target and detect NETs in the NIR region.[37,38] Although these NIR probes have demonstrated effectiveness in detecting and imaging NETs predominantly in vitro and in vivo conditions,[39] the development of low molecular weight NIR probes for staining NETs in pathohistological (ex vivo) samples and for use in flow cytometry remains an intriguing challenge. The size of the probe is one of the crucial factors necessary for attaining high magnification and imparting high-quality images.[40−42] Conventionally, antibody conjugates (IgG and IgM) are often used, but their complex size (typically 150 kDa or ∼1MD) limits the high-resolution structural acquisition. Low molecular weight NIR probes for noninvasive monitoring of NETs have been scarcely reported,[43] with existing solutions often resulting in low resolution and contrast, hindering practical bioimaging applications. The staining of NETs in ex vivo samples enhances the visualization of cellular and subcellular structures and provides deeper insights into disease mechanisms; the detection of NETs via flow cytometry can identify circulating NETs. This could lead to the development of an innovative NIR detection kit for NETs, which would be the first of its kind. Therefore, the creation of low molecular weight NIR probes that can specifically detect NETs in various conditions, including ex vivo applications with superior imaging resolutions and compatibility with flow cytometry, represents a significant advancement in medical diagnostics that has yet to be fully achieved.

With squaraine class of dyes gaining significant traction for bioimaging applications, we reported a benzo[e]indole-based, carboxy-functionalized, unsymmetrical NIR squaraine dye, **SQ-215**, which demonstrated excellent stability and biocompatibility both in vitro and in vivo in mice in our previous work.[44] Building on this foundation, the current study focuses on the detection and imaging of NETs, using rationally designed self-quenching peptide conjugates of **SQ-215**, targeting the protease activity of NE. We have employed both Förster resonance energy transfer (FRET)-based and non-FRET-based probes, incorporating NE-targeting substrates that leverage the protease activity of NE. To ensure specificity for NE in NETs over regular NE in activated neutrophils, the probes were designed to be cell impermeable. The hetero-FRET-based probe, **Hetero-APA**, successfully detected NETs in vitro and in vivo, selectively producing strong fluorescence signals in NET-rich environments when tested in a gout-induced mice model. Meanwhile, the non-FRET probe, **SQ-215-NETP**, which covalently binds to NE, effectively stained NETs in ex vivo samples, achieving an unprecedented image resolution of 90 nm/pixel. Additionally, **SQ-215-NETP** successfully detected NETs in flow cytometry too.

2. MATERIALS AND METHODS

All of the chemicals, solvents, and reagents used for synthesis and photophysical characterizations were of analytical or spectroscopic grade and used as received. All Fmoc protected amino acids, Rink amide MBHA resin, piperidine, coupling reagents HBTU, and HOBt·H_2O, *N*,*N*-diisopropylethylamine (DIPEA), 2,2,2-trifluoroacetic acid (TFA), ethane dithiol, triisopropyl silane, and 4 M HCl/Dioxane were purchased from Watanabe Chemical Industries, Ltd. The proteins, bovine serum albumin (BSA), trypsin from the bovine pancreas, protease (type VIII), α-chymotrypsin (type II), cathepsin from bovine spleen, and thrombin from the bovine and porcine pancreatic elastase, were obtained from Sigma-Aldrich. Deionized water was obtained using a Milli-Q Plus system manufactured by Millipore. The detailed syntheses of squaraine dyes, dye intermediates, and dye-peptide conjugates are elaborated in their respective chapters. Electronic absorption spectra of dye and dye-peptide conjugate in solution were recorded by using a JASCO V-530 UV/vis spectrophotometer, while the fluorescence emission spectrum was recorded by using a JASCO FP-6600 spectrophotometer. The excitation wavelength for all measurements was set at 610 nm, while the default excitation and emission bandwidths were kept at 5 and 2, respectively. When different bandwidths were used, the respective bandwidths are mentioned in the specific experiment. The identities of dyes and dye intermediates were confirmed by HRMS using TOF/FAB-mass in positive ion monitoring mode, while the identities of peptide sequences and dye-peptide conjugates were confirmed by HRMS using a combination of ESI mass in positive ion monitoring mode and MALDI-TOF. The structural elucidation of dyes was done using ^{1}H and ^{13}C nuclear magnetic resonance (NMR) spectroscopy on a JEOL JNM A500 MHz spectrometer in $CDCl_3$ solvent with tetra methyl silane as the internal reference. Analytical high-performance liquid chromatography (HPLC) to estimate the purity of dye-peptide conjugates was conducted using a Hitachi L-7100 instrument equipped with XTerra MS C8 5 μm columns. The mobile phases consisted of 0.1% trifluoroacetic acid (TFA) in H2O (designated as solvent A) and 0.1% TFA in acetonitrile (designated as solvent B). A linear gradient of solvent B in solvent A (ranging from 0% to 50% over 15 min) was employed at a flow rate of 1.0 mL/min. Detection was performed at 254 and 670 nm. Preparative HPLC was performed by using the same instrument but fitted with an Xterra Prep MS C18 OBD 10 μm column. The incubation of the samples was carried out by using an EYELA SLI-400 incubator. Theoretical calculations for the structure optimization of

https://doi.org/10.1021/acsami.4c20658
ACS Appl. Mater. Interfaces 2025, 17, 9140−9154

the dye-peptide conjugates were performed using the Gaussian16 program and Gaussview 6.[45] Optimization parameters include the Hartree−Fock method with 6-31g as the basis set.

3. EXPERIMENTAL SECTION

3.1. Synthesis of Dyes and Dye-Peptide Conjugates. The detailed synthetic procedure, purification, and structural characterization of the dyes and dye-peptide conjugates (probes) are provided in the Supporting Information in Sections S1.1 and S1.2.

3.2. Cell Permeability Studies of the Probes. NK/Ly cells grown in ascites fluid were centrifuged at 1000 g to separate the ascites fluid, followed by suspending the cells in Hanks' balanced salt solution. The probes were added to this solution to a final concentration of 50 nM, incubated at 37 °C during the indicated time, and then put on a slide, covered with a coverslip, and imaged. Imaging the probes was done using fluorescent channels suitable for Cy5.

3.3. Application of the Probes for Vivo Imaging. White laboratory mice of Balb/c line being 12 week-old and weighing 20−25 g were used. Animals were anesthetized and injected intraperitoneally (IP) with 10 μM of the probes in H_2O (containing 1% DMSO) per mouse. Animals were immediately imaged using a LiCor Pearl Trilogy fluorescence analyzer, with excitation using a 685 nm laser and emission at 700 nm channel. The animal studies were approved by the local ethical committee of Danylo Halytsky Lviv National Medical University (Permission 20201221/P9) and conducted according to the guidelines of the Federation of European Laboratory Animal Science Associations (FELASA).

3.4. Fluorescence Microscopy. Fluorescent microscopy was performed as described[46] with an Olympus BX51 fluorescent microscope (Olympus, Tokyo, Japan) equipped with Omega Filters XF407 filter set with excitation at 630/30 nm and emission 710/80 nm (Omega Filters, Brattleboro, USA) and cooled Sony IMX585 sensor-based camera. For NIR imaging, Both 40× 0.75NA, 90× 1.0NA water immersion, and 100× 1.4NA oil immersion objectives were used for live cell imaging. Native Olympus software was used for image processing. Alternatively, a Keyence BZ-X800 fluorescent microscope was used with an appropriate Cy5 fluorescent filter. For image analysis and quantifications, ImageJ software, developed by the National Institutes of Health in Bethesda, MD, USA, was employed. All image analysis tasks were executed using consistent parameters, which included fixed settings for exposure and compensation.

3.5. Kinetic Studies of the Probes with NE in Multiwell Assays. The probes were diluted to a final concentration of 10 μM in either H_2O or phosphate-buffered saline (PBS) with 1% DMSO. 200 μL solution containing the biologically active substance was prepared in 96-well black plates. Either 1 μg of purified murine NE (Lectinotest R&D) or 10 μg of freshly prepared lysate of subcloned Nemeth-Kellner myeloblastoma cells (NK/Ly-RB) overexpressing NE were added to some wells, while others were imaged without NE to evaluate the probe's photostability via photo/autodegradation. Fluorescence emission was studied using PerkinElmer BioAssay reader HST7000 at an excitation of 680/10 nm and emission 720/20 nm at 37 °C or in Li-COR Pearl Trilogy In Vivo imager (LI-COR Biosciences GmbH, Germany) using a 685 nm excitation laser, and emission was analyzed at 700 nm channel, as shown in Figure S17.

3.6. Animals for in Vivo Studies. Studies involving animals, including housing and care, method of euthanasia, and experimental protocols, were approved by the Ethical Committee of Danylo Halytsky Lviv National Medical University, protocols 20191216/10, and 20210622/6, and all experiments were designed to comply with principles of the 3Rs (replacement, reduction, and refinement). Mice were housed in a temperature, humidity, and light controlled environment, with both food and drinking water available ad libitum.

3.7. In Vivo Studies via Air Pouch Model. The air pouch model is a well-established in vivo approach to investigate NETs triggered by monosodium urate (MSU) crystals in mice. Injection of MSU triggers an inflammatory response characterized by neutrophil infiltration into the air pouch leading to the formation of NETs (Figure S18). This model allows for the pouch fluid to be collected for analysis of NET components like citrullinated histone H3, DNA, NE, MPO, and inflammatory mediators.[47,48] Air pouch lavage was isolated by injecting 5 mL of sterile PBS into the air pouch on day 1 and day 3.[49] At day 5, 1 mg of sterile MSU crystals was injected into the air pouch to induce neutrophil infiltration.[50] On day 6, 10 μM of the probes in 1% DMSO solution in water were injected into the air pouch and imaged.

3.8. In Vivo Studies via MSU Crystals-Induced Gout. Gout is chronic inflammatory arthritis characterized by the deposition of MSU crystals in the joints, resulting in intense pain and inflammation, primarily affecting the joints, especially the big toe, ankle, and knee. MSU-induced gout in mice closely resembles the human condition, making it a valuable tool.[51] MSU crystals were prepared at Lectinotest, as previously described.[52] 50 μL portion of a 20 mg/mL suspension of MSU crystals in PBS was injected subcutaneously into the left hind paw, between the metatarsals 2 and 3, while the right paw labeled as controlled was injected with saline. Another mouse was additionally injected ip with 20 mg/kg of proprietary Neutrocure compound 80 (NCure80) (htttp://www.neutrocure.eu) in its left paw aimed at stimulating ROS activity and aggregated NETs formation in vivo[53] resembling gout attack. As a control, the right paw was injected with saline, which did not result in any swelling and hence no gout attack. Measurement of the paw thickness was then conducted using an electronic caliper. Paw images were captured on a cell phone camera for illustrative purposes, as shown in Figure S19.

3.9. Microscopy and Tissue (Ex Vivo) Analysis. Human eye-derived NETs and human coronary thrombi were used for histological assessment of **SQ-215-NETP**. The former was used to make smears on slides and fixed with methanol, and the latter was used to make 7 μm thick Cryosections, fixed in PFA, and stained. 800 nM solution of **SQ-215-NETP** in water was added to tissue samples for 30 min, washed with water, and propidium iodide (PI) at 1 μg/mL was added for another 10 min. The slides were mounted in a wet state in an aqueous mounting medium for fluorescence (Figure S20A) or washed with water, air-dyed, cleared with RotiClear (Carl Roth, DE) organic solution or butanol, and mounted with an organic based xylene-free Roti Mount (Carl Roth, DE) polymeric mounting medium (Figure S20B). Fluorescent microscopy was performed with an Olympus BX51 fluorescent microscope (Olympus, Tokyo, Japan) equipped with an Omega Filters XF407 filter set with excitation at 630/30 nm and emission at 710/80 nm (Omega Filters, Brattleboro, USA) and cooled Sony IMX585 sensor-based camera. NIR imaging was performed with a BZ-X800 microscope (Keyence Corp., Osaka, Japan). Z-stacks were performed to increase the depth of field with a Leica DMI8 motorized microscope using a 40× 1.4 NA oil objective. Z-stacks were performed to increase the depth of field and with a Leica TCS SP5 confocal microscope with 63× 1.45 oil objective. Postprocessing of pictures and morphometry was performed employing Photoshop CS5 64Bit (Adobe, München, Germany), ImageJ, and native microscope software as described in detail.[54]

3.10. Evaluation of Bone Marrow-Derived Neutrophils with Flow Cytometry. Bone marrow was isolated from the mice femur by centrifugation in a 0.5 mL Eppendorf tube for 30 s at maximum speed (13.200 rpm). The cell pellet was lysed for red blood cells in the ammonium buffer for 5 min at 22 °C and washed with 2 mM EDTA, and 2% FBS in PBS buffer. Treatment with 100 nM PMA for 3 h was done to induce NETosis,[55] after which the cells were washed. The formation of NETs upon PMA treatment was confirmed by Sytox staining which confirms DNA externalization from the PMA-treated PMN cells, as shown in Figure S21. Cytometric analysis was performed by using a CytoFLEX Flow Cytometer from Beckmann Coulter (US). Data from the flow cytometry were analyzed with CytExpert version 2.6. For assessment of the mean fluorescence intensity in neutrophils, cells were stained with FITC-conjugated Ly6G (1:200), PE-conjugated CD11a/CD18 (LFA-1) (1:200), and **SQ-215-NETP** (2 μM) for 30 min and then washed in 2% FBS in PBS buffer. DAPI (1 μM) was added to the samples for 5 min, and the cells were washed, suspended in 2% FBS in PBS buffer, and measured. DAPI excitation was done with a 405 nm laser, while **SQ-215-NETP** with a 632 nm laser and detected on the APC channel.

https://doi.org/10.1021/acsami.4c20658
ACS Appl. Mater. Interfaces 2025, 17, 9140−9154

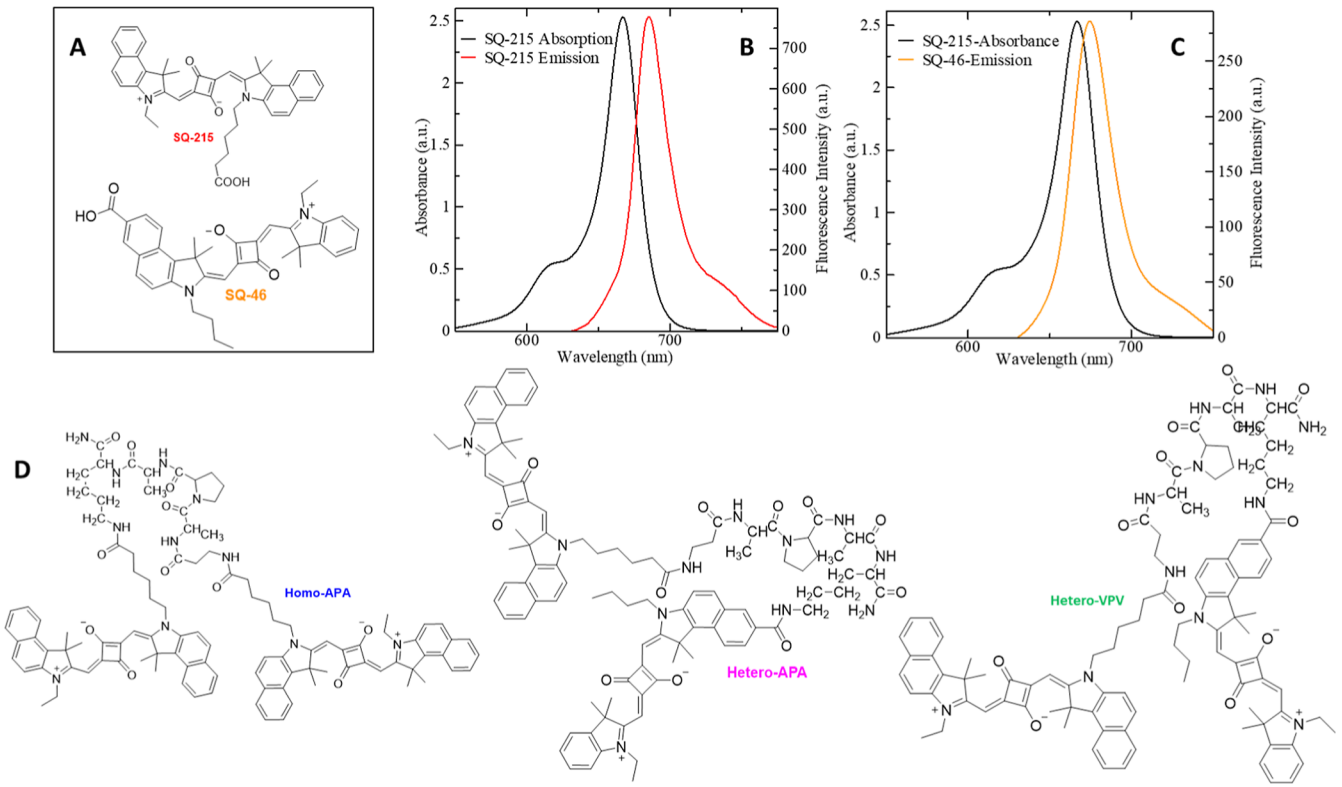

Figure 1. Structure and photophysical characterization of **Homo-APA**; (A) structure of dyes SQ-215 & SQ-46 (fluorophores), (B) overlap of absorption and emission spectra of 10 μM SQ-215 in $CHCl_3$, (C) overlap of absorption and emission spectra of 10 μM of SQ-215 and SQ-46 in $CHCl_3$, and (D) structures of the FRET-based probes.

4. RESULTS AND DISCUSSIONS

4.1. Design and Evaluation of FRET-Based Probes.

FRET-based probes provide high sensitivity for detecting protease activity due to their ability to generate fluorescence signals in response to proteolytic cleavage and their ability to monitor protease activity in real-time. Upon proteolytic cleavage, FRET-based probes change fluorescence properties, allowing for the continuous monitoring of protease activity kinetics, thereby providing valuable insights into protease-regulated processes under various physiological or pathological conditions. FRET-based probes can be designed to specifically target and respond to proteases of interest by incorporating a protease recognition sequence or substrate into the probe design. Therefore, the first endeavor was to incorporate the NE recognition sequence. In designing the recognition sequence for NE, we selected the tripeptide *Ala-Pro-Ala* (APA) as the substrate based on NE's known substrate specificity. NE generally cleaves substrates after small aliphatic amino acids, including Alanine (Ala, A), Valine (Val, V), and Isoleucine (Ile, I), in the P1 position on the C-terminal side.[56,57] While other sequences, such as AAPL and AAPV, have been widely studied, our group had briefly investigated the substrate *APA* in the context of enzyme recognition and hydrolysis, though its full potential as a probe especially in vitro, in vivo, and ex vivo has not at all been explored.[58] This work expands on *APA's* unique attributes, both by delving into its performance in vitro, in vivo and ex vivo conditions as a recognition unit and by optimizing the FRET system to enhance probe sensitivity and specificity. Having two Ala residues sandwiched with a proline residue in the substate allows for more cleavage sites for NE on the C-terminal side of the individual Ala residues. The shorter *APA* sequence also allowed us to further explore its potential as a more compact substrate that could maintain high specificity while improving probe design simplicity. This choice leverages the fundamental substrate preferences of NE and provides a unique and untested peptide for efficient NE recognition.

FRET probes typically consist of a donor and acceptor moiety on either end of the peptide recognition unit within the Foster radius, leading to fluorescence quenching. The dye **SQ-215,** depicted in Figure 1A, was chosen as both the donor and acceptor unit owing to its small Stokes shift of only 20 nm allowing the significant overlap of the absorption and emission spectra of **SQ-215,** as shown in Figure 1B, leading to the design of the Homo-FRET system. On the other hand, for the Hetero-FRET system, **SQ-46** (Figure 1A), an analogous dye of **SQ-215**, with a relatively smaller Stokes shift reducing the gap between absorption and emission maxima up to 10 nm was designed and synthesized. A perusal of Figure 1C corroborates the enhanced overlap between the emission spectra of **SQ-46** and the absorption spectra of **SQ-215** as compared to the homo-FRET. β-Ala and Lys were added as spacers to facilitate the coupling of **SQ-215** and **SQ-46** into the NE recognition sequence as well as to impart the optimal access of the NE to the recognition unit consisting of a tripeptide. Thus, two *Ala-Pro-Ala*-based probes **Homo-APA** and **Hetero-APA** (Figure 1D) were designed, synthesized, and characterized photophysically, in which the hetero system turned out to perform better than the Homo system owing to the enhanced absorption and emission spectral overlapping. The probes were found to be self-quenching owing to FRET and aggregation-caused quenching (ACQ) mechanisms (Supporting Information S2.2 and S2.4). The probe is designed with a donor−acceptor FRET pair, positioned to facilitate efficient energy transfer between the

https://doi.org/10.1021/acsami.4c20658
ACS Appl. Mater. Interfaces 2025, 17, 9140−9154

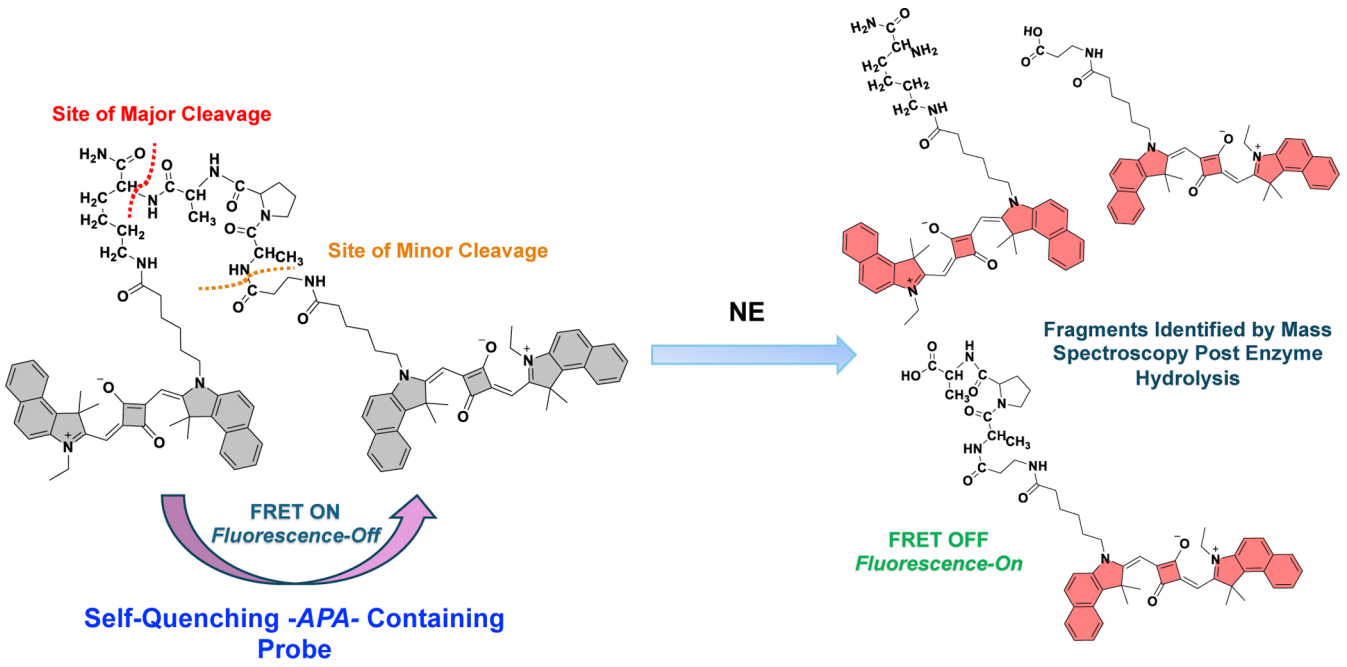

Figure 2. Schematic diagram elucidating the mechanism behind the reappearance of the fluorescence signal in the presence of NE.

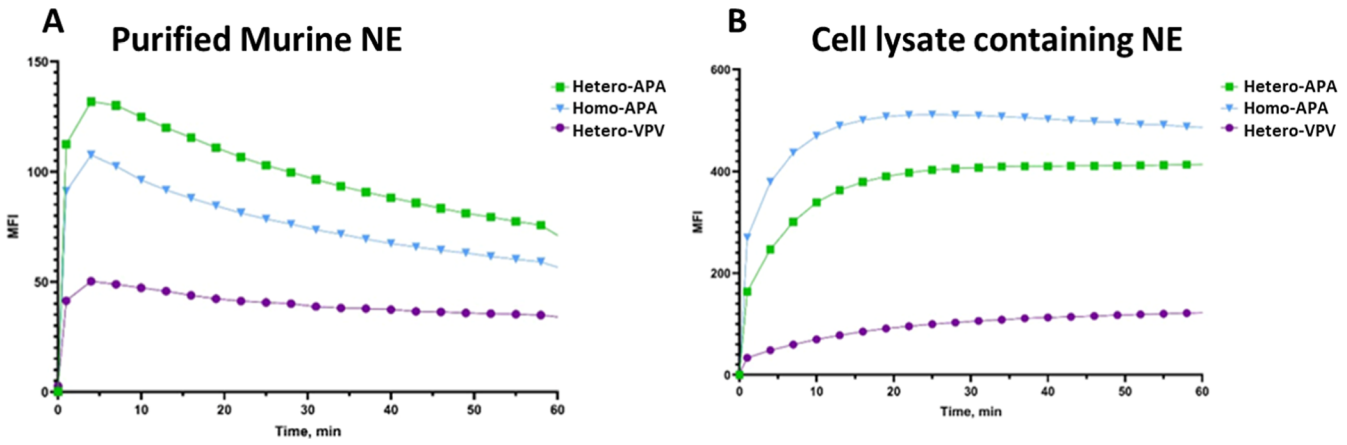

Figure 3. Kinetics study showing the changes in fluorescence intensities of the probes upon the addition of (A) 1 μg of purified murine NE and (B) freshly prepared lysate of NK/Ly-RB cells overexpressing NE.

fluorophores when in close proximity. This proximity is achieved through the specific peptide sequence *Ala-Pro-Ala*, which serves as the recognition site for NE. Our analysis using mass spectrometry identified that NE majorly cleaves the probe precisely between the Ala on the C-terminal and Lys residues (Figure S24), while also slightly cleaving between the β-Ala on the C-terminal and the Ala residues, which are located adjacent to the recognition site. In the absence of NE, this FRET-based design maintains a fluorescence-off state, as the close distance between the donor and acceptor fluorophores promotes energy transfer, which quenches the donor fluorescence. Additionally, aggregation of probe molecules further contributes to quenching through ACQ. Upon addition of NE, however, the enzyme specifically recognizes the *Ala-Pro-Ala* sequence and cleaves at the Lys−Ala bond by unleashing its protease activity. This cleavage disrupts the proximity of the donor and acceptor, preventing energy transfer and thus restoring the fluorescence (Figure 2). This NE-mediated release of fluorescence confirms the effective design of the probe, as it enables fluorescence activation specifically in response to the target enzyme, enhancing detection specificity.

To study the effect of the change on the hydrophobicity and size of the aliphatic amino acid in the probe toward the reactivity of NE, another hetero-FRET probe **Hetero-VPV** based on *Val-Pro-Val* as the NE recognition sequence was also synthesized (Figure 1D). The FRET-based probes were then evaluated for the specific detection of NETs.

4.1.1. In Vitro Investigation of Homo and Hetero FRET-Based Probes. All three FRET-based probes were first treated with purified murine NE and freshly prepared lysate of subcloned Nemeth-Kellner myeloblastoma (NK/Ly-RB) cells overexpressing NE in black 96-well plates, and their respective fluorescent kinetics were monitored over a period of 1 h to study the probe's sensitivity toward NE, as shown in Figure 3.

A perusal of Figure 3 clearly shows that probes are in the fluorescent-off state but regained fluorescence and show a significant increase in the fluorescence intensity upon the addition of NE or cell lysate containing NE. The probes

https://doi.org/10.1021/acsami.4c20658
ACS Appl. Mater. Interfaces 2025, 17, 9140−9154

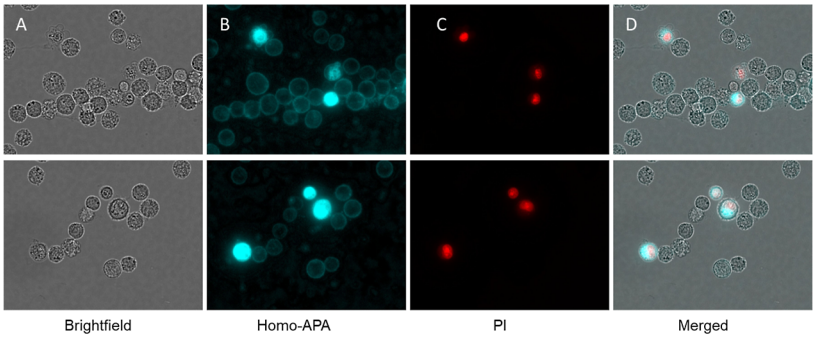

Figure 4. Fluorescence emission of Homo-APA with lysed NK/Ly-RB cells overexpressing NE (A) Brightfield image, (B) NIR signal from Homo-APA, (C) cells stained with PI, (D) merged image showing the overlapping of the NIR signal and PI signal. Exi: 625/25 nm, Emi: 700/40 nm for (B), and Exi: 560/20 nm, Emi: 630/30 nm for (C).

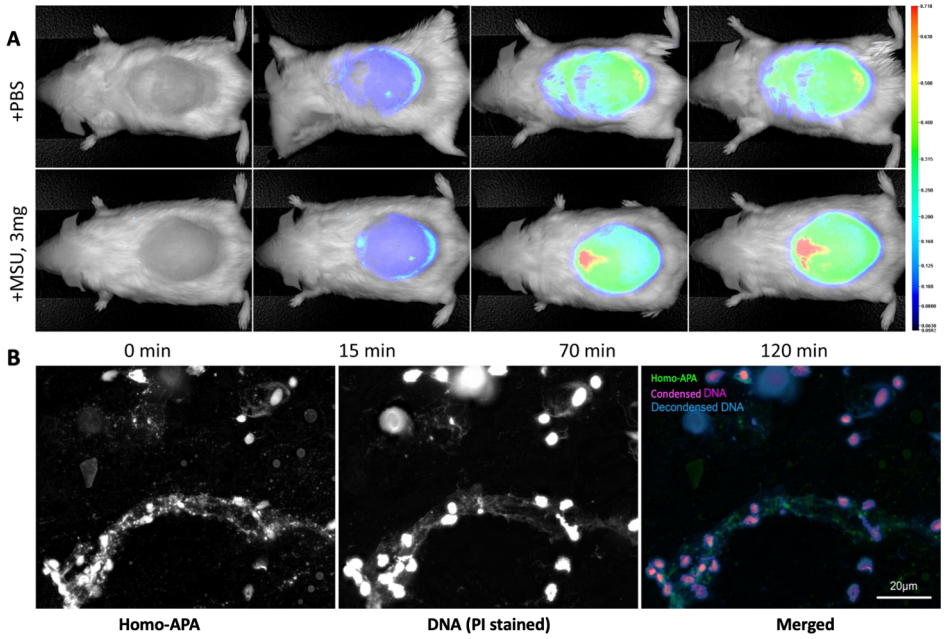

Figure 5. (A) Fluorescence dynamics of **Homo-APA** in the air pouch of mice containing PBS as control (top row) and MSU (bottom row). (B) Contents of the air pouch under microscopy showing **Homo-APA** signal interspersed with DNA confirming the detection of NETs.

containing the *Ala-Pro-Ala* sequence demonstrated better activity toward NE compared to the *Val-Pro-Val* containing probe. Among the *Ala-Pro-Ala* probes, **Hetero-APA** showed better activity than **Homo-APA** with purified murine NE, while **Homo-APA** showed a slight improvement in the activity in the case of cell lysate containing NE. Among purified NE (Figure 3A) and cell lysate containing NE (Figure 3B), both the *Ala-Pro-Ala* probes exhibited higher fluorescent intensity with the cell lysate than purified NE. Both **Hetero-APA** and **Homo-APA** showed nearly 4-fold higher increases in fluorescence intensity with the cell lysate containing NE than purified NE. On the other hand, **Hetero-VPV** showed similar activity with both purified NE and cell lysate containing NE.

To sense and image NETs, cell permeability becomes a crucial parameter. As NETs are formed as an extracellular matrix, it becomes even more important for the probes to be cell impermeable. Also, NE is found in neutrophils during the degranulation process. Therefore, there is a need to design cell-impermeable probes to detect NETs and NE in inflamed tissues and the microenvironment. Considering this, the cell permeability of **Homo-APA** was investigated. 10 μM **Homo-APA** was treated with live NK/Ly-RB cells overexpressing NE, and the fluorescence emission was monitored under microscopy, and no fluorescence was observed (Figure 4A). To further conclude that the probe is cell-impermeable and produces the signal only in the presence of NE, the cells were lysed to expose the inner contents. Cells were treated with 10% ethanol to lyse the cells, and the fluorescence behavior was observed under microscopy upon the addition of 10 μM of **Homo-APA,** as shown in Figure 4.

Figure 4B shows a fluorescence signal emanating from some of the cells post 10% ethanol addition. To affirm the signal that is coming is indeed from the necrotic cells, the cells were stained with PI, a membrane-impermeable fluorescent dye used for DNA staining.[59] Since lysed cells have their DNA exposed, staining with PI is a good indicator of cell death. Figure 4C shows the fluorescence emission of PI bound to DNA. Upon merging both the fluorescence images of **Homo-APA** and PI (Figure 4D), it is evident that the fluorescence signal is indeed emanating from lysed cell overexpressing NE. Thus, **Homo-APA** is cell impermeable and produces signals only in the presence of NE, rendering these probes fluorescent-on only in the presence of NE. With encouraging results from in vitro

https://doi.org/10.1021/acsami.4c20658
ACS Appl. Mater. Interfaces 2025, 17, 9140−9154

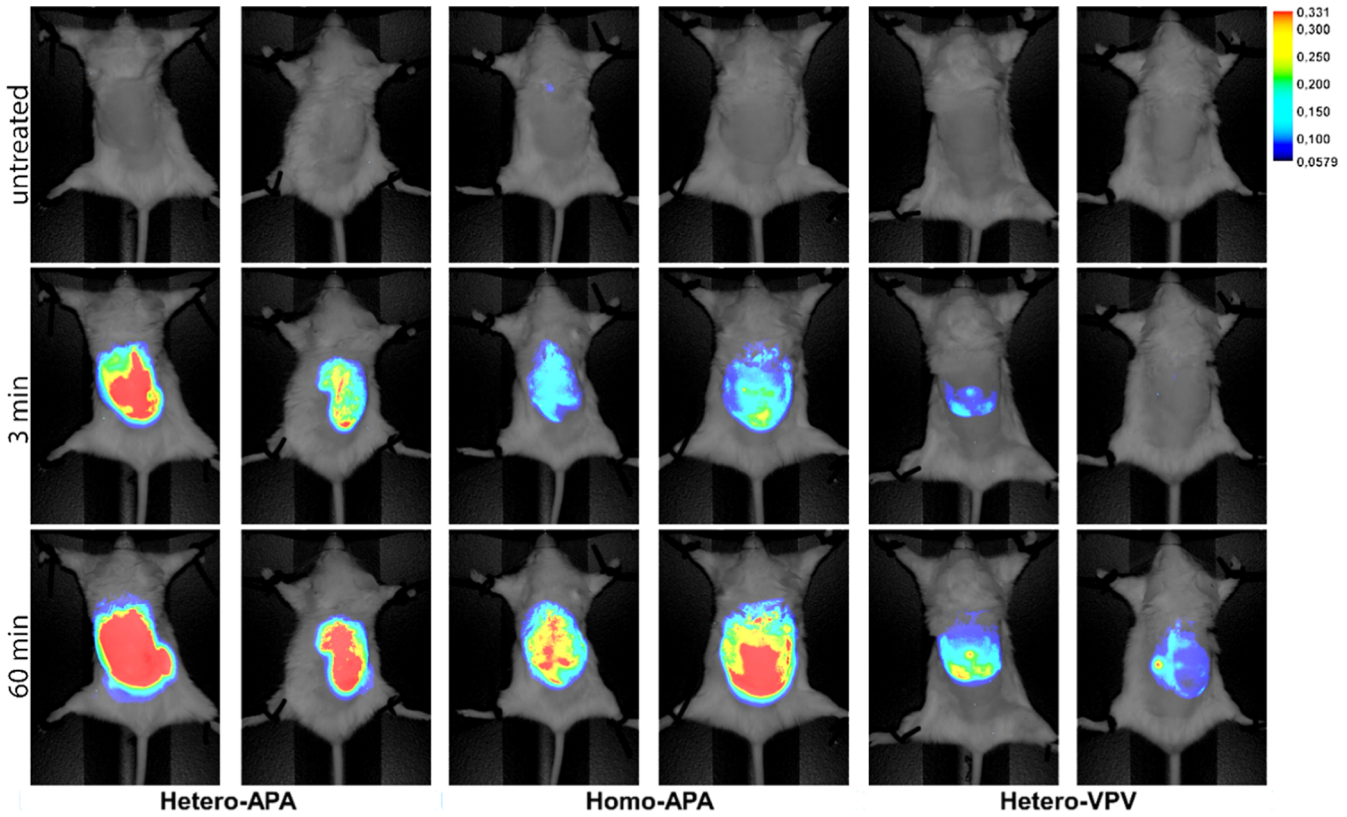

Figure 6. In vivo comparison of FRET-based probes in the air pouch with MSU-induced NETs.

studies, the probes were then tested in vivo in NET-induced laboratory mice.

4.1.2. In Vivo Investigation of Homo and Hetero FRET-Based Probes. The in vivo studies were carried out using the air pouch model. 10 μM **Homo-APA** was injected into the created air pouches of two white balb/c mice. While in the control mice, PBS was injected, the other mice were injected with 3 mg of MSU. The fluorescence dynamics were measured using live in vivo imaging at 700 nm, as shown in Figure 5A.

A perusal of Figure 5A shows no significant fluorescence signal in the air pouch with PBS of the control mice, whereas a strong and intense signal is observed in the MSU-injected mice. To clarify that the signal was indeed due to NETs, the contents of the air pouch were extracted, transferred to slides, fixed, and observed under microscopy, as shown in Figure 5B. Microscopic images revealed the formation of NETs in the MSU-injected mice. NETs, characterized by condensed and decondensed DNA, are observed with PI staining. Our finding confirms that the probe is in a fluorescent-off state in the absence of NE and becomes fluorescent-on in the presence of NE, rendering the probe highly specific toward NE in NETs coupled with the cell-impermeable nature of the probe. The dye-only control for all in vivo studies has been omitted to remove the redundancy. The in vivo behavior of **SQ-215** and other similar squaraine dyes has been extensively studied and published in our previous studies.[44,60] The dyes themselves, when injected into mice, do not contribute to FRET or any form of quenching. The dyes-only show stable and strong fluorescence in vivo. Thus, the quenching of the probes in vivo is solely attributed to the rational probe design. Furthermore, all three probes were compared for their efficiency in vivo with the same MSU-induced NETs formation in the air pouch models, which are summarized in Figure 6. Two mice per group (probe) were used for this study.

A perusal of Figure 6 clearly shows that **Hetero-APA** displays better efficiency among the various probes. On the other hand, **Hetero-VPV** containing the *Val-Pro-Val* sequence displayed the least activity for NE. This reiterates the preference for *Ala* over *Val* for the interaction of the NE with the probe. All of the probes showed neither toxicity nor behavioral changes in mice. Evaluation of cell cytotoxicity of the probes using flow cytometry confirmed that relatively high concentration of these probes did not exhibit any significant cytotoxic effects (Supporting Information section S4, Figure. S30).

Hetero-APA, the best-performing probe, was further tested in a gout-induced mice model. 1 μM **Hetero-APA** was injected into IP, and the fluorescence dynamics were monitored. As shown in Figure 7, the left paw of mouse A with MSU mimics slight inflammation, whereas mice B was injected with MSU and propriety PMN-dependent ROS-enhancer NCure80, which further activates the neutrophils mimicking the gout condition.

It can be observed from Figure 7 that the probe **Hetero-APA** produced a strong fluorescence signal in the gout-induced paw (Figure 7B,L) compared to the MSU only injected paw (Figure 7A,L). In the right paws of both mice with saline as control, a significant signal was seen. Thus, we conclude that **Hetero-APA** not only exhibits good activity in vitro and in vivo in the air pouch models but also in diseased states characterized by chronic inflammation by locating and accumulating in these microenvironments.

4.2. Design and Characterization of Non-FRET-Based Probe SQ-215-NETP. While FRET-based *Ala-Pro-Ala* probes exhibited promising efficacy in detecting the NETs, their performance was compromised in ex vivo samples. The accurate sensing and imaging of ex vivo specimens are pivotal for early disease detection, prognosis assessment, and treatment monitoring. To address this limitation and develop a more

https://doi.org/10.1021/acsami.4c20658
ACS Appl. Mater. Interfaces 2025, 17, 9140−9154

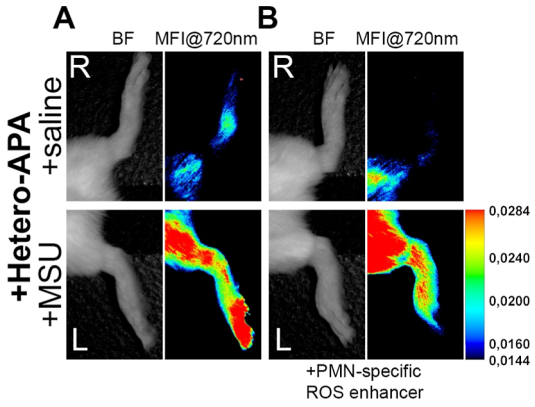

Figure 7. Study on the Gout-induced mice model. IP injection of **Hetero-APA** into **mice A**: left paw (L) with 3 mg of MSU and the right paw (R) with saline; and **mice B:** left paw with 20 mg/kg MSU & NCure80 to induce gout and right paw with saline.

effective probe for detection of NETs in ex vivo samples, an alternative approach was pursued, and hence, NE's regulation in the human system was studied. The interplay between the NE and human α1-antitrypsin (AAT) stands as a fundamental regulatory mechanism in the proteolytic cascade governing inflammatory responses and tissue homeostasis.[61,62] AAT, a member of the serine protease inhibitor (Serpin) superfamily, serves as the primary endogenous inhibitor of NE. Structurally, AAT adopts a metastable conformation, rendering itself susceptible to proteolytic attack by NE. Upon encountering NE, AAT undergoes a conformational change, transitioning from the native state to an acylenzyme intermediate complex. This transformation involves the insertion of the reactive center loop (RCL) of AAT, as a bait, into the active site of NE, leading to the formation of a covalent bond between the serine residue of NE and the methionine residue at position 358 of AAT.[63−65] AAT is known to exhibit a remarkable degree of specificity toward NE, over other serine proteases.[66] Thus, to target NE on NETs, we designed a non-FRET probe **SQ-215-NETP,** as shown in Figure 8A, consisting of a polypeptide chain based on the 13 amino acids sequence (*GEAIPMSIPPEVK*) derived from the RCL of AAT. The fluorophore **SQ-215** and *GEAIPMSIPPEVK* were connected by a polyethylene glycol spacer.

To assess the probe's specificity, 10 μM **SQ-215-NETP** in PBS was incubated with BSA and other serine proteases at 25 °C, followed by monitoring of the fluorescence dynamics for 30 min. As seen in Figure 8B, the addition of high concentrations of proteases and BSA did not lead to any significant increase in fluorescence intensity. The peptide sequence *GEAIPMSIPPEVK* is known to be highly specific to NE, binding covalently without undergoing cleavage, as previously reported by Michelle A. Cruz et al.[67] **SQ-215-NETP** was further examined in vitro and in vivo to establish and validate its specificity toward NE and as a potential candidate for sensing and imaging NETs.

4.2.1. In Vitro Evaluation of ***SQ-215-NETP.*** **SQ-215-NETP** was treated with purified murine NE and freshly prepared lysate of NK/Ly-RB cells overexpressing NE in black 96-well plates, and their respective fluorescent kinetics were monitored over 1 h and compared to that of **Hetero-APA,** as shown in Figure 9.

As observed with the FRET-based probes, **SQ-215-NETP** showed good efficiency with both the cell lysate containing NE and purified NE over **Hetero-APA**. However, the absolute amount of fluorescence in two experimental setups cannot be compared, as purified NE can lose some activity, and the amount of NE expressed in cells is difficult to determine. However, the probe was shown to be completely cell-nonpermeable, making it an ideal marker for externalized NE, as seen during NETosis induction. **SQ-215-NETP** overall performed much better than the **Hetero-APA. SQ-215-NETP** showed more than 3-fold higher fluorescence intensity with purified NE and nearly 10-fold higher intensity with cell lysate containing NE compared to

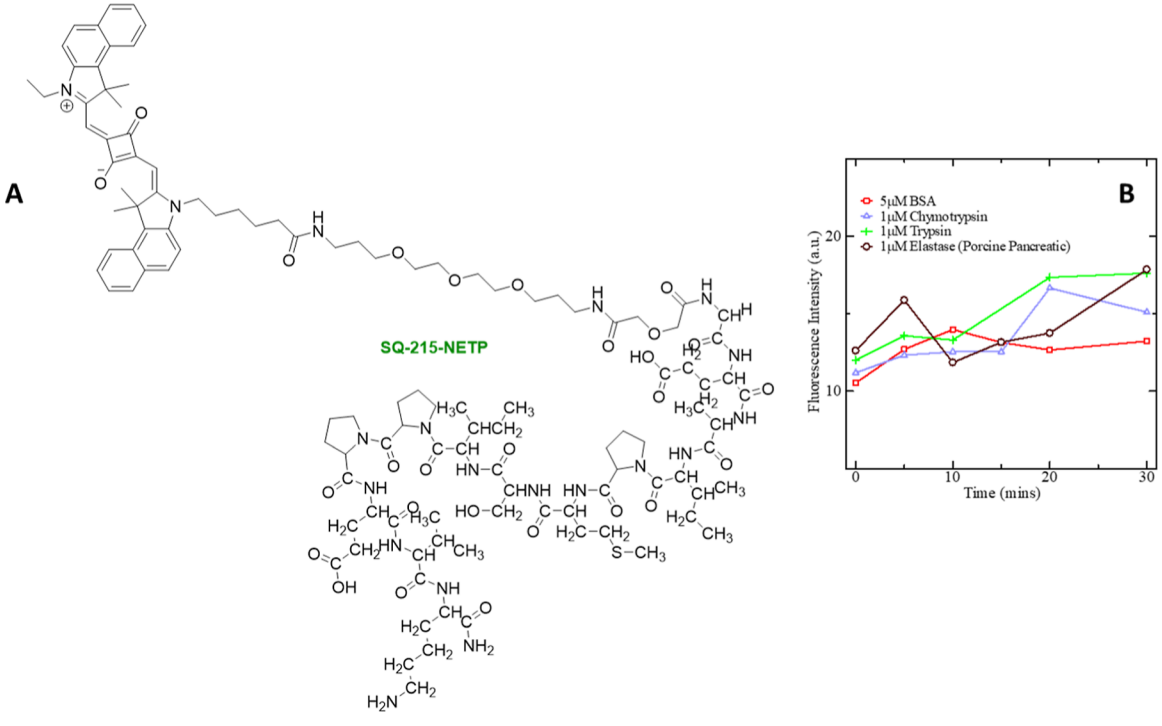

Figure 8. Structure (A) and specificity (B) of **SQ-215-NETP**.

https://doi.org/10.1021/acsami.4c20658
ACS Appl. Mater. Interfaces 2025, 17, 9140−9154

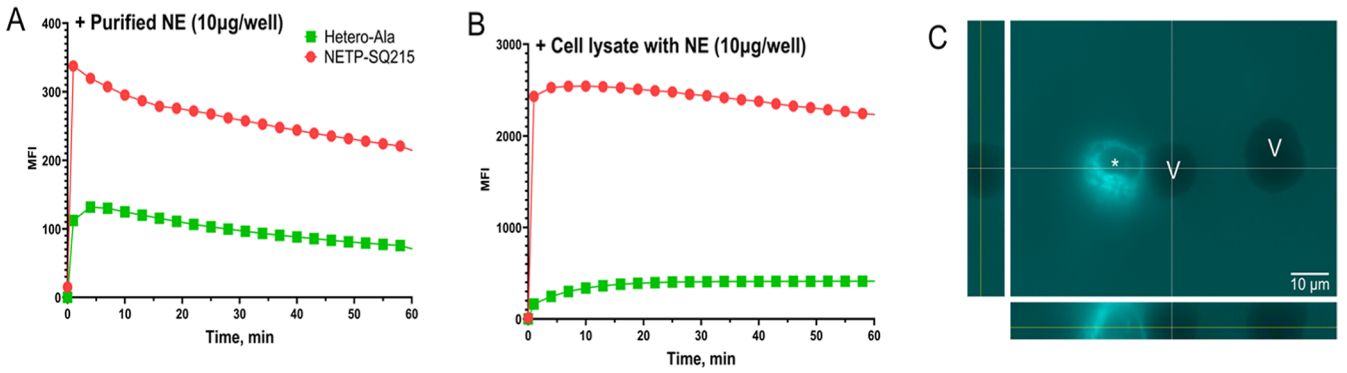

Figure 9. Kinetics study of **SQ-215-NETP** showing the change in fluorescence intensity upon the addition of (A) purified murine NE, (B) freshly prepared lysate of NK/Ly-RB cells overexpressing NE, and (C) cell permeability study showing **SQ-215-NETP** penetration only into dying NK/Ly-RB cells (marked × after addition of 10% EtOH for 10 min) and not into viable (V) cells.

Hetero-APA (Figure 9A,B). Subsequently, **SQ-215-NETP** was directly studied in gout-induced mice models in vivo.

*4.2.2. In Vivo Evaluation of **SQ-215-NETP**.* Gout was induced using the same procedure mentioned previously. 1 μM of **SQ-215-NETP** was injected IP in both mice, and fluorescence dynamics was measured, as shown for 4 h post-treatment in Figure 10.

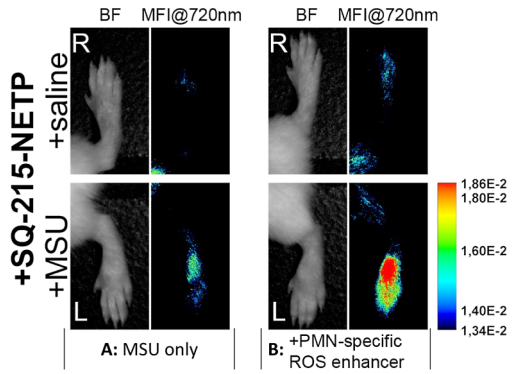

Figure 10. IP injection of **SQ-215-NETP** in MSU-induced gout inflammation: **mice A**: left paw (L) with MSU and the right paw (R) with saline; **mice B**: left paw with MSU & additional NCure80 to induce gout and right paw with saline.

No fluorescent signal was seen in the right paws of both mice (Figure 10; top row). A stable and strong fluorescence signal can be seen in the gout-induced left paw (Figure 10B,L). This shows **SQ-215-NETP**'s ability to localize in inflamed tissues and accumulate only in the microenvironment of NETs formation. Like **Hetero-APA, SQ-215-NETP** also displayed selective accumulation in an inflamed microenvironment with the fluorescence signal emanating from the protease activity of NE, along with showing no toxicity (Supporting Information section S4, Figure. S30) or behavioral change in mice. With higher sensitivity toward NE than **Hetero-APA, SQ-215-NETP** was further tested in different ex vivo samples.

*4.2.3. Evaluation of **SQ-215-NETP** on Pathohistological Samples.* The newly designed **SQ-215-NETP** offers 2-fold benefits such as its efficient binding with the target imparting high resolution, and its smaller size below 5 kDa allows the facile removal of nonbonded substances by kidneys. This interest led us to test the **SQ-215-NETP** utilizing various pathohistological samples like NETs derived from human mucosal surfaces (human eyes) and human thrombi. The best histological slide mounting system was selected at the first stage. It was noticed that the use of water-based mounting systems (RotiMount Aqua) resulted in blurred images after slide storage for 3 days (Figure S20A). The use of the organic (oil-based) mounting system RotiMount (Carl Roth, DE) resulted in high-resolution clear imaging preserving fluorescence at least for one month while they were retested (Figure S20B). Thus, this system was selected for all further experiments.

To explore the resolution limits of NE detection with **SQ-215-NETP**, human coronary thrombi were imaged with conventional fluorescent microscopy with z-stack employing a 20× (Figure 11A) and high-NA 40× 1.4NA objective (Figure

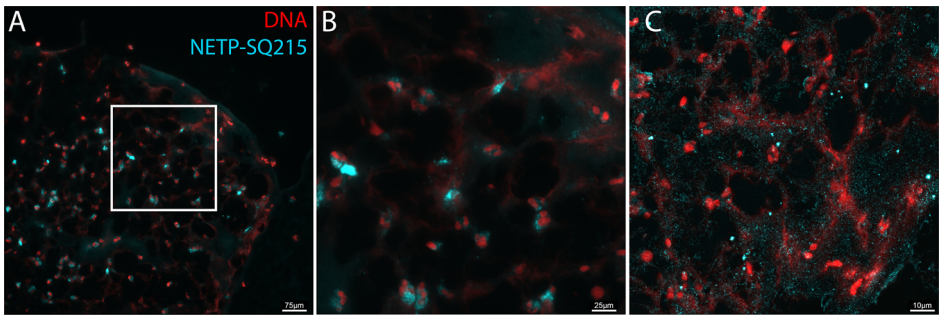

Figure 11. Fluorescent microscopy of human coronary thrombi; (A) fluorescent wide field scan of NETs derived from the human coronary thrombi in the presence of 800 nM **SQ-215-NETP**; (B) fluorescent microscopy of the indicated field within A with increased depth of field; (C) confocal scan of the corresponding area demonstrated that the blurred signals are due to specific NE-positive granules of DNA fibers. (**Blue: SQ-215-NETP** at 700 nm and **red:** PI staining showing DNA).

https://doi.org/10.1021/acsami.4c20658
ACS Appl. Mater. Interfaces 2025, 17, 9140−9154

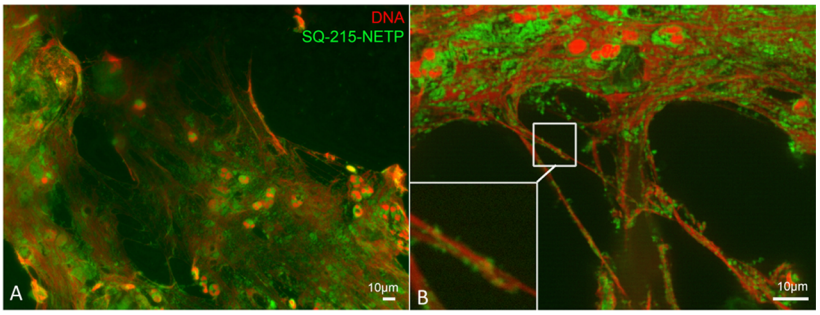

Figure 12. Evaluation of **SQ-215-NETP** in human NETs from the mucosal surface using fluorescent microscopy only (A) and those combined with optical sectioning techniques (B).

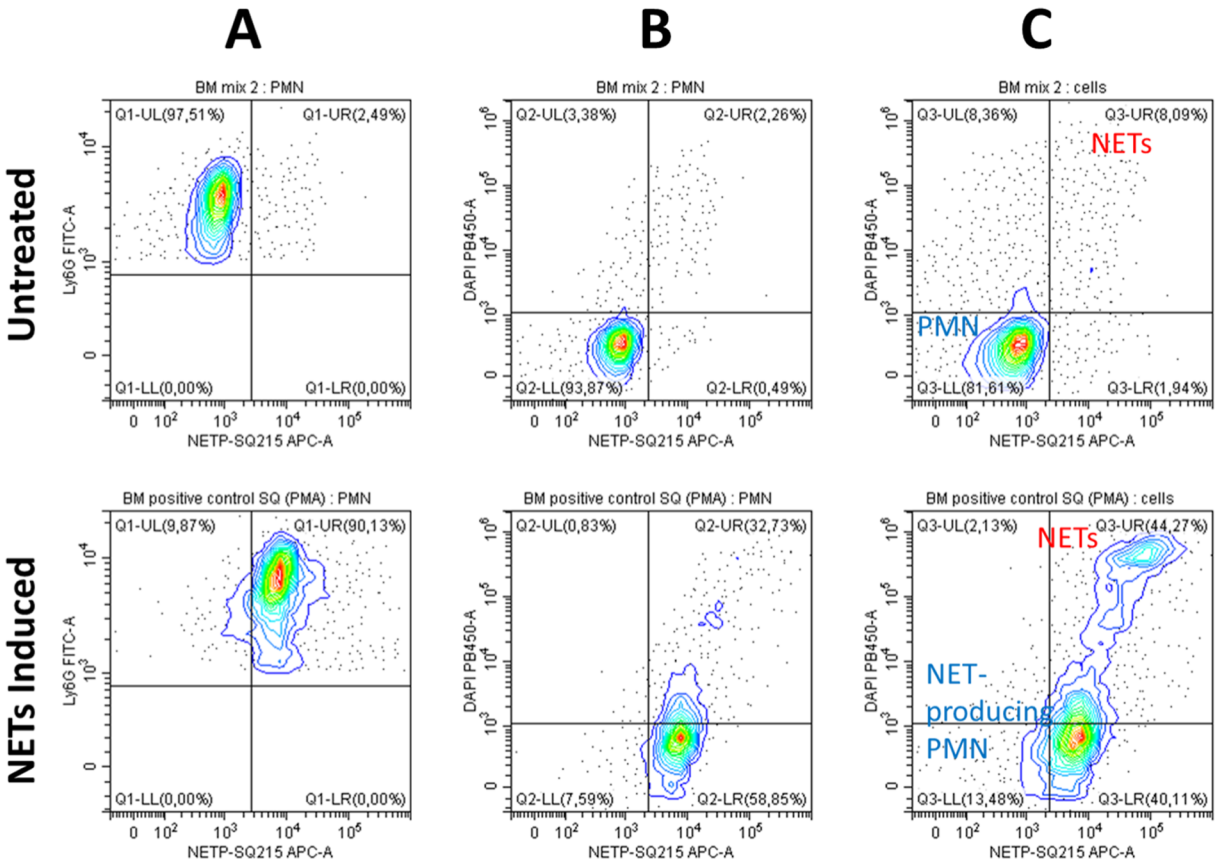

Figure 13. Flow cytometry analysis of mice bone marrow stained with **SQ-215-NETP**; **top row:** before (untreated) and **bottom row:** after strong induction of NETs. [(A,B) are gated on neutrophils (Ly6G+), while (C) is gated on all bone marrow cells].

11B). Where NETosis found around DNA released from neutrophil cells (judged by nuclei morphology) was accompanied by "clouds" of the NE-positive signal coming from **SQ-215-NETP**, some big granules with NE were seen inside neutrophils or in the vicinity of their place of NETosis formation. Further analysis of "NE-positive clouds" using confocal scanning microscopy revealed a set of small NE granules decorating externalized DNA, as typically assumed to be a classical NETosis feature. The resolution limit achieved was around 100 nm/pixel and was limited by microscopic resolutions. Figure 11C shows the spread-out signal of **SQ-215-NETP** emanating from the binding to NE and the red stain representing the DNA. The diffused signal due to NE at the areas of nuclear destruction at a high resolution is visualized as a set of granules over the decondensed DNA (red). The small size of the **SQ-215-NETP** molecule allowed us to achieve such an unprecedented high resolution for granule discrimination (around 100 nm/pixel).

SQ-215-NETP was also successfully used to stain the NETs derived from the mucosal surface. Here to achieve high-resolution, structured-illumination optical sectioning fluorescent microscopy was employed to achieve a resolution around 90 nm/pixel (Figure 12).

Figure 12B clearly shows the visualization of NE deposits on DNA fibrils. The DNA fibers are stained in red, while the signal from **SQ-215-NETP** due to NE binding is shown in green. Generally, achieving such a high resolution is challenging in ex vivo samples. Thus, **SQ-215-NETP** covalent binding to NE resulted in achieving greater accuracy in microscopy. Both confocal scanning and structured-illumination optical sectioning fluorescent microscopy generally require superb photostability of the dye. No significant signal loss was observed on slides after

https://doi.org/10.1021/acsami.4c20658
ACS Appl. Mater. Interfaces 2025, 17, 9140−9154

a series of scans using both methods (Figure 12A,B), suggesting the high photostability of the **SQ-215** fluorophore.

*4.2.4. Evaluation of **SQ-215-NETP** in Flow Cytometry.* Flow cytometry is crucial for disease biomarker detection, as this technique is highly sensitive and capable of detecting low-abundance biomarkers with high specificity due to the use of fluorescently labeled probes. Flow cytometry provides quantitative data, allowing for the precise measurement of biomarker levels, which is crucial for accurate disease diagnosis and monitoring. The size of the probe used in flow cytometry can significantly impact the quality of the results. Smaller probes provide better penetration and binding to target biomarkers, resulting in higher signal-to-noise ratios and more accurate detection. Larger molecular weight probes can suffer from steric hindrance, reducing their ability to access target sites and potentially decreasing the signal intensity. Low molecular weight NIR probes offer several advantages for disease biomarker detection in flow cytometry in terms of reduced background fluorescence, deeper tissue penetration, and enhanced multiplexing capabilities.

Mice bone marrow was stained with **SQ-215-NETP** before and after strong induction of NETs using PMA for 3 h. The NIR signal was monitored by excitation using a 632 nm laser and detected by using a standard APC channel (650/20 nm). The results are depicted in Figure 13.

Figure 13A shows cells gated on Ly6G, a marker specific to PMN (neutrophils) on the *Y*-axis and **SQ-215-NETP** on the *X*-axis. After NETs are induced, particles positive for both the Ly6G marker and **SQ-215-NETP** are found abundantly in the upper right quadrangle. This indicates that the neutrophils show a positive NIR signal from **SQ-215-NETP** after the induction of NETosis. Now to specifically detect NETs, DNA was marked with DAPI, and its signal was seen to be that of **SQ-215-NETP**. Figure 13B is gated on Ly6G + cells (PMN) and indicates that after the induction of NETs, the neutrophils slowly become DAPI and **SQ-215-NETP** positive, indicating the beginning of NETosis, i.e., neutrophils starting to produce NETs. Figure 13C is gated on all cellular events, and it clearly shows a large number of particles positive for NETs in the upper right quadrangle as indicated by the DAPI and **SQ-215-NETP** staining (formed NETs), while more neutrophils forming NETs are seen below. Thus, **SQ-215-NETP** also allows for monitoring NETs in a flow cytometry setup which opens the potential for detecting circulating NETs in clinical samples.

In conclusion, **SQ-215-NETP** allows for the continuous detection of NETs by binding to active (and fixed in samples) NE with great resolution. Due to the long-lasting nature of NETs within inflamed tissues, even minor protease activity detected in time may have profound physiological and therapeutic consequences. Therefore, the new reporters bear the potential to generate a comprehensive picture of NETs-mediated inflammatory processes, functional links among extracellular DNA content, protease activity in inflamed microenvironments, and disease prognosis.

5. CONCLUSIONS

This work addresses the need for advanced detection and imaging of the NETs, crucial biomarkers in various inflammatory diseases, COVID-19-related lung injury, cardiovascular conditions, and cancers. We have developed novel self-quenching and cell-impermeable NIR fluorescent probes based on squaraine dye-peptide conjugates, leveraging the protease activity of NE, for the real-time detection and imaging

Table 1. Detailed Comparison of SQ-215-NETP with Previously Reported NET Imaging Probes

parameters	SQ-215-NETP (this work)	antibody-based probe[68]	nanoparticle-based probe[69]	tandem-locked NETosis reporter[43] (TNR1)	protease FRET reporter[38] (H-NE)	small molecule-based[70]
probe type	small molecule dye-peptide conjugate (non-FRET)	monoclonal antibody 2C5	functionalized nanoparticles (NH_2–PEG–CdSe (ZnS) Qdots)	tandem peptide-based activatable fluorescent probe	FRET-based-peptide-Hoechst conjugate	DNA-chelating fluorescent dye
detection target	covalently binds to neutrophil elastase (NE)	nucleosomes present in NETs	NETs	neutrophil elastase (NE) and cathepsin G (CTSG)	DNA-bound NE	extracellular DNA
specificity	high (100% NE-specific)	moderate	high	dual enzyme specificity (but requires CTSG cleavage also for NETs detection)	high for DNA-bound NE	moderate
resolution	~100 nm (high-resolution ex vivo)	50 μm	~20 μm	100 μm (ex-vivo)	100 μm (Mouse lung slices) 10 μm [Cystic Fibrosis (CF) sputum]	50 μm (ex vivo)
in vivo applicability	yes (tested in gout-induced mice model)	NA	NA	yes (NETosis monitoring in tumor-bearing mice)	NA	NA
ex vivo applicability	yes (FFPE and cryosections)	NA	NA	yes	yes (lung tissue, CF patient sputum)	yes
flow cytometry compatibility	yes	NA	NA	NA	NA	NA
clinical relevance	high (applicable to sepsis, cancer, COVID-19, cardiovascular specimens)	limited	Limited	high (immunotherapy prognosis in cancer patients)	high (CF inflammation and DNA-bound protease detection)	limited

https://doi.org/10.1021/acsami.4c20658
ACS Appl. Mater. Interfaces 2025, 17, 9140−9154

of NETs. Among the FRET-based probes, **Hetero-APA** was highly specific toward NETs in both in vitro and in vivo studies. **Hetero-APA** was able to effectively detect and image NETs in inflammatory environments when tested in a gout-induced mice. Though **Hetero-APA** allowed direct visualization of NETs in vivo but was not suitable for ex vivo samples, leading to the development of the non-FRET probe **SQ-215-NETP** that covalently binds to NE. **SQ-215-NETP** resulted in high-resolution imaging and stability in ex vivo samples, including human coronary thrombi and mucosal samples, achieving resolutions up to 90 nm/pixel. Further, **SQ-215-NETP** was also able to detect NETs in flow cytometry as well, opening the possibility to quantitatively evaluate NETs in blood samples, in conditions where NE activity is detrimental like sepsis & COVID-19.

Table 1 shows the comparison of **SQ-215-NETP** with previously reported NET imaging probes, highlighting **SQ-215-NETP's** superior performance across key parameters with multiple imaging modalities. **SQ-215-NETP** demonstrates exceptional performance in all categories, especially its high resolution in ex vivo conditions, unique compatibility with flow cytometry, and high specificity for NE. Other probes show limitations in resolution, sensitivity, or applicability to multiple modalities. This study highlights significant advancements in NETs detection and imaging, emphasizing the high specificity and biocompatibility of the probes. These probes can be utilized to enhance the understanding of NETs/NE-mediated inflammatory processes, and **SQ-215-NETP** offers promising tools for improved diagnostic and therapeutic strategies in managing inflammatory diseases and cancers.

■ ASSOCIATED CONTENT

Supporting Information

The Supporting Information is available free of charge at https://pubs.acs.org/doi/10.1021/acsami.4c20658.

Synthesis, purification, and photophysical characterization of squaraine dyes and dye-peptide conjugates; NMR, HPLC, and mass spectroscopy data of SQ-46 and dye-peptide conjugates; elucidation of cleavage site and mechanism for FRET-based probes; fluorescence quenching mechanisms for FRET-based probes and SQ-215-NETP; evaluation of cytotoxicity of the probes; statistical data/quantification of fluorescence intensities for in vivo imaging; figures for fluorescence kinetics of all the probes in multiwell assay; MSU-induced NETs formation in the mouse air pouch model; mice paw swelling showing MSU-induced gout attack; best slid mounting condition for ex vivo imaging of SQ-215-NETP; and Sytox Green staining confirming the formation of NETosis post PMA treatment (PDF)

■ AUTHOR INFORMATION

Corresponding Authors

Sai Kiran Mavileti − *Graduate School of Life Science and System Engineering, Kyushu Institute of Technology, 808-0196 Kitakyushu, Japan;* orcid.org/0009-0001-4164-158X; Email: m.c.saikiran.sai25@gmail.com

Rostyslav Bilyy − *Lectinotest R&D, 79000 Lviv, Ukraine; Department of Histology, Cytology & Embryology, Danylo Halytsky Lviv National Medical University, 79010 Lviv, Ukraine; Institute of Cellular Biology and Pathology "Nicolae Simionescu", 050568 Bucharest, Romania;* orcid.org/0000-0002-2344-1349; Email: r.bilyy@gmail.com

Shyam S. Pandey − *Graduate School of Life Science and System Engineering, Kyushu Institute of Technology, 808-0196 Kitakyushu, Japan;* orcid.org/0000-0001-8102-1003; Email: shyam@life.kyutech.ac.jp

Authors

Galyna Bila − *Lectinotest R&D, 79000 Lviv, Ukraine; Department of Histology, Cytology & Embryology, Danylo Halytsky Lviv National Medical University, 79010 Lviv, Ukraine; Institute of Cellular Biology and Pathology "Nicolae Simionescu", 050568 Bucharest, Romania;* orcid.org/0000-0002-8084-8268

Valentyn Utka − *Lectinotest R&D, 79000 Lviv, Ukraine*

Rostyslav Bilyy, Jr. − *Lectinotest R&D, 79000 Lviv, Ukraine*

Evgenia Bila − *Lectinotest R&D, 79000 Lviv, Ukraine; Department of Organic Chemistry, Ivan Franko National University of Lviv, 79005 Lviv, Ukraine*

Elena Butoi − *Institute of Cellular Biology and Pathology "Nicolae Simionescu", 050568 Bucharest, Romania*

Shekhar Gupta − *Graduate School of Life Science and System Engineering, Kyushu Institute of Technology, 808-0196 Kitakyushu, Japan*

Priyanka Balyan − *Graduate School of Life Science and System Engineering, Kyushu Institute of Technology, 808-0196 Kitakyushu, Japan*

Tamaki Kato − *Graduate School of Life Science and System Engineering, Kyushu Institute of Technology, 808-0196 Kitakyushu, Japan*

Complete contact information is available at: https://pubs.acs.org/10.1021/acsami.4c20658

Author Contributions

#**S.K.M.** and **G.B.** contributed equally by conceptualization, investigation, resources, data curation, and formal analysis. **S.K.M** prepared the original draft. **V.U., E.B., Ev.Bi., El.Bu., R.B.Jr., S.G., P.B., and T.K.** contributed by resources, assisting in experiments, and preparing figures and tables. **R.B.** and **S.S.P.** contributed equally by conceptualization, validation, investigation, resources, writing−review and editing, supervision, and project administration.

Funding

This work was financially supported by the European Union's Horizon 2020 research and innovation program under grant agreement No 872331 NoBiasFluors ⟨⟨Nonbiased fluorescent dyes as markers of drugs for optical in cellular and in vivo imaging⟩⟩ and 101129095 "LungCare", Simons Foundation Grants 1037973 and 1290588 to EB, EFIS Ukraine Mobility Initiative to RB, and NextGeneration EU call PNRR−III-C9−2022-I8−93 Grant 760063 HeartCure. In vivo, imaging facilities used in the current research were established under the Grant of National Research Foundation of Ukraine 2020.02/0131.

Notes

The authors declare no competing financial interest.

■ ACKNOWLEDGMENTS

Authors S.K.M. and S.S.P. thank the Ministry of Education, Culture, Sports, Science and Technology (MEXT), Govt. of Japan for providing the doctoral scholarship to S.K.M. The authors thank Prof. Andriy Mokhir and NeutroCure consortium for providing neutrophil-specific activator compounds, Maria

Anghelache for assistance with flow cytometry, Andreea Mihaila for neutrophil handling, and Mihai Melnic for providing clinical samples.

REFERENCES

(1) Burn, G. L.; Foti, A.; Marsman, G.; Patel, D. F.; Zychlinsky, A. The Neutrophil. *Immunity* **2021**, *54* (7), 1377−1391.
(2) Kolaczkowska, E.; Kubes, P. Neutrophil Recruitment and Function in Health and Inflammation. *Nat. Rev. Immunol.* **2013**, *13* (3), 159−175.
(3) Burgener, S. S.; Schroder, K. Neutrophil Extracellular Traps in Host Defense. *Cold Spring Harb Perspect Biol.* **2020**, *12* (7), a037028.
(4) Papayannopoulos, V.; Metzler, K. D.; Hakkim, A.; Zychlinsky, A. Neutrophil Elastase and Myeloperoxidase Regulate the Formation of Neutrophil Extracellular Traps. *J. Cell Biol.* **2010**, *191* (3), 677−691.
(5) Pham, C. T. N. Neutrophil Serine Proteases: Specific Regulators of Inflammation. *Nat. Rev. Immunol.* **2006**, *6* (7), 541−550.
(6) Korkmaz, B.; Moreau, T.; Gauthier, F. Neutrophil Elastase, Proteinase 3 and Cathepsin G: Physicochemical Properties, Activity and Physiopathological Functions. *Biochimie* **2008**, *90* (2), 227−242.
(7) Owen, C. Leukocyte Cell Surface Proteinases: Regulation of Expression, Functions, and Mechanisms of Surface Localization. *Int. J. Biochem. Cell Biol.* **2008**, *40* (6−7), 1246−1272.
(8) Herdendorf, T. J.; Geisbrecht, B. V. Investigation of Human Neutrophil Elastase Inhibition by Staphylococcus Aureus EapH1: The Key Role Played by Arginine 89. *Biochemistry* **2018**, *57* (50), 6888−6896.
(9) Anderson, B. M.; Poole, D. P.; Aurelio, L.; Ng, G. Z.; Fleischmann, M.; Kasperkiewicz, P.; Morissette, C.; Drag, M.; van Driel, I. R.; Schmidt, B. L.; Vanner, S. J.; Bunnett, N. W.; Edgington-Mitchell, L. E. Application of a Chemical Probe to Detect Neutrophil Elastase Activation during Inflammatory Bowel Disease. *Sci. Rep.* **2019**, *9* (1), 13295.
(10) Voynow, J. A.; Shinbashi, M. Neutrophil Elastase and Chronic Lung Disease. *Biomolecules* **2021**, *11* (8), 1065.
(11) Wan, J.; Ren, Y.; Yang, X.; Li, X.; Xia, L.; Lu, N. The Role of Neutrophils and Neutrophil Extracellular Traps in Acute Pancreatitis. *Front. Cell Dev. Biol.* **2021**, *8*, 565758.
(12) Sarkar, S.; Shil, A.; Nandy, M.; Singha, S.; Reo, Y. J.; Yang, Y. J.; Ahn, K. H. Rationally Designed Two-Photon Ratiometric Elastase Probe for Investigating Inflammatory Bowel Disease. *Anal. Chem.* **2022**, *94* (2), 1373−1381.
(13) Shi, Y.; Dong, M.; Wu, Y.; Gong, F.; Wang, Z.; Xue, L.; Su, Z. An Elastase-Inhibiting, Plaque-Targeting and Neutrophil-Hitchhiking Liposome against Atherosclerosis. *Acta Biomater.* **2024**, *173*, 470−481.
(14) Fujii, M.; Miyagi, Y.; Bessho, R.; Nitta, T.; Ochi, M.; Shimizu, K. Effect of a Neutrophil Elastase Inhibitor on Acute Lung Injury after Cardiopulmonary Bypass. *Interact. Cardiovasc. Thorac. Surg.* **2010**, *10* (6), 859−862.
(15) Ishii, T.; Doi, K.; Okamoto, K.; Imamura, M.; Dohi, M.; Yamamoto, K.; Fujita, T.; Noiri, E. Neutrophil Elastase Contributes to Acute Lung Injury Induced by Bilateral Nephrectomy. *Am. J. Pathol.* **2010**, *177* (4), 1665−1673.
(16) Hoenderdos, K.; Condliffe, A. The Neutrophil in Chronic Obstructive Pulmonary Disease. Too Little, Too Late or Too Much, Too Soon? *Am. J. Respir. Cell Mol. Biol.* **2013**, *48* (5), 531−539.
(17) Papayannopoulos, V. Neutrophil Extracellular Traps in Immunity and Disease. *Nat. Rev. Immunol.* **2018**, *18* (2), 134−147.
(18) Wigerblad, G.; Kaplan, M. J. Neutrophil Extracellular Traps in Systemic Autoimmune and Autoinflammatory Diseases. *Nat. Rev. Immunol.* **2023**, *23* (5), 274−288.
(19) Mauracher, L.-M.; Posch, F.; Martinod, K.; Grilz, E.; Däullary, T.; Hell, L.; Brostjan, C.; Zielinski, C.; Ay, C.; Wagner, D. D.; Pabinger, I.; Thaler, J. Citrullinated Histone H3, a Biomarker of Neutrophil Extracellular Trap Formation, Predicts the Risk of Venous Thromboembolism in Cancer Patients. *J. Thromb. Haemostasis* **2018**, *16* (3), 508−518.
(20) Scozzi, D.; Liao, F.; Krupnick, A. S.; Kreisel, D.; Gelman, A. E. The Role of Neutrophil Extracellular Traps in Acute Lung Injury. *Front. Immunol.* **2022**, *13*, 953195.
(21) Narasaraju, T.; Neeli, I.; Criswell, S. L.; Krishnappa, A.; Meng, W.; Silva, V.; Bila, G.; Vovk, V.; Serhiy, Z.; Bowlin, G. L.; Meyer, N.; Luning Prak, E. T.; Radic, M.; Bilyy, R. Neutrophil Activity and Extracellular Matrix Degradation: Drivers of Lung Tissue Destruction in Fatal COVID-19 Cases and Implications for Long COVID. *Biomolecules* **2024**, *14* (2), 236.
(22) Arcanjo, A.; Logullo, J.; Menezes, C. C. B.; de Souza Carvalho Giangiarulo, T. C.; dos Reis, M. C.; de Castro, G. M. M.; da Silva Fontes, Y.; Todeschini, A. R.; Freire-de-Lima, L.; Decoté-Ricardo, D.; Ferreira-Pereira, A.; Freire-de-Lima, C. G.; Barroso, S. P. C.; Takiya, C.; Conceição-Silva, F.; Savino, W.; Morrot, A. The Emerging Role of Neutrophil Extracellular Traps in Severe Acute Respiratory Syndrome Coronavirus 2 (COVID-19). *Sci. Rep.* **2020**, *10* (1), 19630.
(23) Kim, S.-H.; Kim, J.; Jang, J. Y.; Noh, H.; Park, J.; Jeong, H.; Jeon, D.; Uhm, C.; Oh, H.; Cho, K.; Jeon, Y.; On, D.; Yoon, S.; Lim, S.-Y.; Kim, S. P.; Lee, Y. W.; Jang, H. J.; Park, I. H.; Oh, J.; Seo, J. S.; Kim, J. J.; Seok, S.-H.; Lee, Y. J.; Hong, S.-M.; An, S.-H.; Kim, S. Y.; Kim, Y. B.; Hwang, J.-Y.; Lee, H.-J.; Kim, H. B.; Choi, K.-S.; Park, J. W.; Seo, J.-Y.; Yun, J.-W.; Shin, J.-S.; Lee, H.-Y.; Kim, K.; Lee, D.; Lee, H.; Nam, K. T.; Seong, J. K. Mouse Models of Lung-Specific SARS-CoV-2 Infection with Moderate Pathological Traits. *Front. Immunol.* **2022**, *13*, 1055811.
(24) Porto, B. N.; Stein, R. T. Neutrophil Extracellular Traps in Pulmonary Diseases: Too Much of a Good Thing? *Front. Immunol.* **2016**, *7*, 311.
(25) Szturmowicz, M.; Demkow, U. Neutrophil Extracellular Traps (NETs) in Severe SARS-CoV-2 Lung Disease. *Int. J. Mol. Sci.* **2021**, *22* (16), 8854.
(26) Shao, B.-Z.; Yao, Y.; Li, J.-P.; Chai, N.-L.; Linghu, E.-Q. The Role of Neutrophil Extracellular Traps in Cancer. *Front. Oncol.* **2021**, *11*, 714357.
(27) Lerman, I.; Hammes, S. R. Neutrophil Elastase in the Tumor Microenvironment. *Steroids* **2018**, *133*, 96−101.
(28) Yang, L.; Liu, Q.; Zhang, X.; Liu, X.; Zhou, B.; Chen, J.; Huang, D.; Li, J.; Li, H.; Chen, F.; Liu, J.; Xing, Y.; Chen, X.; Su, S.; Song, E. DNA of Neutrophil Extracellular Traps Promotes Cancer Metastasis via CCDC25. *Nature* **2020**, *583* (7814), 133−138.
(29) Albrengues, J.; Shields, M. A.; Ng, D.; Park, C. G.; Ambrico, A.; Poindexter, M. E.; Upadhyay, P.; Uyeminami, D. L.; Pommier, A.; Küttner, V.; Bružas, E.; Maiorino, L.; Bautista, C.; Carmona, E. M.; Gimotty, P. A.; Fearon, D. T.; Chang, K.; Lyons, S. K.; Pinkerton, K. E.; Trotman, L. C.; Goldberg, M. S.; Yeh, J. T.-H.; Egeblad, M. Neutrophil Extracellular Traps Produced during Inflammation Awaken Dormant Cancer Cells in Mice. *Science* **2018**, *361* (6409), No. eaao4227.
(30) Tan, X.; Luo, S.; Wang, D.; Su, Y.; Cheng, T.; Shi, C. A NIR Heptamethine Dye with Intrinsic Cancer Targeting, Imaging and Photosensitizing Properties. *Biomaterials* **2012**, *33* (7), 2230−2239.
(31) Licha, K.; Welker, P.; Weinhart, M.; Wegner, N.; Kern, S.; Reichert, S.; Gemeinhardt, I.; Weissbach, C.; Ebert, B.; Haag, R.; Schirner, M. Fluorescence Imaging with Multifunctional Polyglycerol Sulfates: Novel Polymeric near-IR Probes Targeting Inflammation. *Bioconjug. Chem.* **2011**, *22* (12), 2453−2460.
(32) Meador, W. E.; Autry, S. A.; Bessetti, R. N.; Gayton, J. N.; Flynt, A. S.; Hammer, N. I.; Delcamp, J. H. Water-Soluble NIR Absorbing and Emitting Indolizine Cyanine and Indolizine Squaraine Dyes for Biological Imaging. *J. Org. Chem.* **2020**, *85* (6), 4089−4095.
(33) MacCuaig, W. M.; Wickizer, C.; Van, R. S.; Buabeng, E. R.; Lerner, M. R.; Grizzle, W. E.; Shao, Y.; Henary, M.; McNally, L. R. Influence of Structural Moieties in Squaraine Dyes on Optoacoustic Signal Shape and Intensity. *Chem.* **2024**, *10* (2), 713−729.
(34) Lv, C.; Xia, T.; Zhang, H.; Liu, W.; Zhao, X.; Yang, M.; Du, J.; Sun, W.; Fan, J.; Peng, X. A Non-Peptide-Based Chemiluminescent Probe for Sensitively Visualizing Neutrophil Elastase Activity in Vivo. *Dyes Pigm.* **2023**, *220*, 111741.
(35) Liu, S.-Y.; Xiong, H.; Li, R.-R.; Yang, W.-C.; Yang, G.-F. Activity-Based Near-Infrared Fluorogenic Probe for Enabling in Vitro and in

https://doi.org/10.1021/acsami.4c20658
ACS Appl. Mater. Interfaces 2025, 17, 9140−9154

Vivo Profiling of Neutrophil Elastase. *Anal. Chem.* **2019**, *91* (6), 3877−3884.
(36) Huang, L.; Su, W.; Zhu, L.; Li, J.; Quan, W.; Yoon, J.; Lin, W. A Biocompatible Probe for the Detection of Neutrophil Elastase Free from the Interference of Structural Changes and Its Application to Ratiometric Photoacoustic Imaging In Vivo. *Angew. Chem., Int. Ed.* **2023**, *62* (9), No. e202217508.
(37) Rodriguez-Rios, M.; Rinaldi, G.; Megia-Fernandez, A.; Lilienkampf, A.; Robb, C. T.; Rossi, A. G.; Bradley, M. Moving into the Red − a near Infra-Red Optical Probe for Analysis of Human Neutrophil Elastase in Activated Neutrophils and Neutrophil Extracellular Traps. *Chem. Commun.* **2023**, *59* (78), 11660−11663.
(38) Guerra, M.; Halls, V. S.; Schatterny, J.; Hagner, M.; Mall, M. A.; Schultz, C. Protease FRET Reporters Targeting Neutrophil Extracellular Traps. *J. Am. Chem. Soc.* **2020**, *142* (48), 20299−20305.
(39) Hao, Y.; Liu, D.; Wang, K.; Liu, Q.; Chen, H.; Ji, S.; Ding, D. Imaging and Therapy of Tumors Based on Neutrophil Extracellular Traps. *Small Sci.* **2024**, *4*, 2400212.
(40) Sahl, S. J.; Hell, S. W.; Jakobs, S. Fluorescence Nanoscopy in Cell Biology. *Nat. Rev. Mol. Cell Biol.* **2017**, *18* (11), 685−701.
(41) Wang, L.; Frei, M. S.; Salim, A.; Johnsson, K. Small-Molecule Fluorescent Probes for Live-Cell Super-Resolution Microscopy. *J. Am. Chem. Soc.* **2019**, *141* (7), 2770−2781.
(42) Seah, D.; Cheng, Z.; Vendrell, M. Fluorescent Probes for Imaging in Humans: Where Are We Now? *ACS Nano* **2023**, *17* (20), 19478−19490.
(43) Cheng, P.; He, S.; Zhang, C.; Liu, J.; Pu, K. A Tandem-Locked Fluorescent NETosis Reporter for the Prognosis Assessment of Cancer Immunotherapy. *Angew. Chem., Int. Ed.* **2023**, *62* (26), No. e202301625.
(44) Mavileti, S. K.; Bila, G.; Utka, V.; Bila, E.; Kato, T.; Bilyy, R.; Pandey, S. S. Photophysical Characterization and Biointeractions of NIR Squaraine Dyes for in Vitro and in Vivo Bioimaging. *ACS Appl. Bio Mater.* **2024**, *7* (1), 416−428.
(45) Frisch, M. J.; Trucks, G. W.; Schlegel, H. B.; Scuseria, G. E.; Robb, M. A.; Cheeseman, J. R.; Scalmani, G.; Barone, V.; Petersson, G. A.; Nakatsuji, H. *G16_C01. Gaussian 16*. Revision C. 01; Gaussian. Inc.: Wallin, 2016, p 248.
(46) Bila, G.; Schneider, M.; Peshkova, S.; Krajnik, B.; Besh, L.; Lutsyk, A.; Matsyura, O.; Bilyy, R. Novel Approach for Discrimination of Eosinophilic Granulocytes and Evaluation of Their Surface Receptors in a Multicolor Fluorescent Histological Assessment. *Ukrainian Biochem. J.* **2020**, *92* (2), 99−106.
(47) Wang, Y.; Du, C.; Zhang, Y.; Zhu, L. Composition and Function of Neutrophil Extracellular Traps. *Biomolecules* **2024**, *14* (4), 416.
(48) Bruschi, M.; Petretto, A.; Santucci, L.; Vaglio, A.; Pratesi, F.; Migliorini, P.; Bertelli, R.; Lavarello, C.; Bartolucci, M.; Candiano, G.; Prunotto, M.; Ghiggeri, G. M. Neutrophil Extracellular Traps Protein Composition Is Specific for Patients with Lupus Nephritis and Includes Methyl-Oxidized Aenolase (Methionine Sulfoxide 93). *Sci. Rep.* **2019**, *9* (1), 7934.
(49) Bilyy, R.; Paryzhak, S.; Turcheniuk, K.; Dumych, T.; Barras, A.; Boukherroub, R.; Wang, F.; Yushin, G.; Szunerits, S. Aluminum Oxide Nanowires as Safe and Effective Adjuvants for Next-Generation Vaccines. *Mater. Today* **2019**, *22*, 58−66.
(50) Pieterse, E.; Jeremic, I.; Czegley, C.; Weidner, D.; Biermann, M. H. C.; Veissi, S.; Maueröder, C.; Schauer, C.; Bilyy, R.; Dumych, T.; Hoffmann, M.; Munoz, L. E.; Bengtsson, A. A. A.; Schett, G.; van der Vlag, J.; Herrmann, M. Blood-Borne Phagocytes Internalize Urate Microaggregates and Prevent Intravascular NETosis by Urate Crystals. *Sci. Rep.* **2016**, *6* (1), 38229.
(51) Pieterse, E.; Jeremic, I.; Czegley, C.; Weidner, D.; Biermann, M. H. C.; Veissi, S.; Maueröder, C.; Schauer, C.; Bilyy, R.; Dumych, T.; Hoffmann, M.; Munoz, L. E.; Bengtsson, A. A.; Schett, G.; van der Vlag, J.; Herrmann, M. Blood-Borne Phagocytes Internalize Urate Microaggregates and Prevent Intravascular NETosis by Urate Crystals. *Sci. Rep.* **2016**, *6* (1), 38229.
(52) Schauer, C.; Janko, C.; Munoz, L. E. L. E.; Zhao, Y. Y.; Kienhöfer, D.; Frey, B.; Lell, M.; Manger, B.; Rech, J.; Naschberger, E.; Holmdahl, R.; Krenn, V.; Harrer, T.; Jeremic, I.; Bilyy, R.; Schett, G.; Hoffmann, M.; Herrmann, M. Aggregated Neutrophil Extracellular Traps Limit Inflammation by Degrading Cytokines and Chemokines. *Nat. Med.* **2014**, *20* (5), 511−517.
(53) Daum, S.; Reshetnikov, M. S. V.; Sisa, M.; Dumych, T.; Lootsik, M. D.; Bilyy, R.; Bila, E.; Janko, C.; Alexiou, C.; Herrmann, M.; Sellner, L.; Mokhir, A. Lysosome-Targeting Amplifiers of Reactive Oxygen Species as Anticancer Prodrugs. *Angew. Chem., Int. Ed.* **2017**, *56* (49), 15545−15549.
(54) Bila, G.; Vishchur, O.; Vovk, V.; Vari, S.; Bilyy, R. Neutrophil Activation at High-Fat High-Cholesterol and High-Fructose Diets Induces Low-Grade Inflammation in Mice. *Ukrainian Biochem. J.* **2024**, *96* (2), 27−37.
(55) Hoppenbrouwers, T.; Autar, A. S. A.; Sultan, A. R.; Abraham, T. E.; van Cappellen, W. A.; Houtsmuller, A. B.; van Wamel, W. J. B.; van Beusekom, H. M. M.; van Neck, J. W.; de Maat, M. P. M. In Vitro Induction of NETosis: Comprehensive Live Imaging Comparison and Systematic Review. *PLoS One* **2017**, *12* (5), No. e0176472.
(56) Fu, Z.; Thorpe, M.; Akula, S.; Chahal, G.; Hellman, L. T. Extended Cleavage Specificity of Human Neutrophil Elastase, Human Proteinase 3, and Their Distant Ortholog Clawed Frog PR3-Three Elastases With Similar Primary but Different Extended Specificities and Stability. *Front. Immunol.* **2018**, *9*, 2387.
(57) Lefkowitz, R. B.; Schmid-Schönbein, G. W.; Heller, M. J. Whole Blood Assay for Elastase, Chymotrypsin, Matrix Metalloproteinase-2, and Matrix Metalloproteinase-9 Activity. *Anal. Chem.* **2010**, *82* (19), 8251−8258.
(58) Saikiran, M.; Sato, D.; Pandey, S. S.; Hayase, S.; Kato, T. Efficient near Infrared Fluorescence Detection of Elastase Enzyme Using Peptide-Bound Unsymmetrical Squaraine Dye. *Bioorg. Med. Chem. Lett.* **2017**, *27* (17), 4024−4029.
(59) Belloc, F.; Dumain, P.; Boisseau, M. R.; Jalloustre, C.; Reiffers, J.; Bernard, P.; Lacombe, F. A Flow Cytometric Method Using Hoechst 33342 and Propidium Iodide for Simultaneous Cell Cycle Analysis and Apoptosis Determination in Unfixed Cells. *Cytometry* **1994**, *17* (1), 59−65.
(60) Priyanka; Bila, G.; Mavileti, S. K.; Bila, E.; Negrych, N.; Gupta, S.; Tang, L.; Bilyy, R.; Pandey, S. S.; Kato, T. A Biocompatible NIR Squaraine Dye and Dye-Antibody Conjugates for Versatile Long-Term In Vivo Fluorescence Bioimaging. *Mater. Adv.* **2024**, *5*, 3940.
(61) Janciauskiene, S. M.; Bals, R.; Koczulla, R.; Vogelmeier, C.; Köhnlein, T.; Welte, T. The Discovery of A1-Antitrypsin and Its Role in Health and Disease. *Respir. Med.* **2011**, *105* (8), 1129−1139.
(62) Owen, C. A.; Campbell, M. A.; Sannes, P. L.; Boukedes, S. S.; Campbell, E. J. Cell Surface-Bound Elastase and Cathepsin G on Human Neutrophils: A Novel, Non-Oxidative Mechanism by Which Neutrophils Focus and Preserve Catalytic Activity of Serine Proteinases. *J. Cell Biol.* **1995**, *131* (3), 775−789.
(63) Elliott, P. R.; Lomas, D. A.; Carrell, R. W.; Abrahams, J. P. Inhibitory Conformation of the Reactive Loop of A1-Antitrypsin. *Nat. Struct. Mol. Biol.* **1996**, *3* (8), 676−681.
(64) Elliott, P. R.; Pei, X. Y.; Dafforn, T. R.; Lomas, D. A. Topography of a 2.0 Å Structure of α 1 -antitrypsin Reveals Targets for Rational Drug Design to Prevent Conformational Disease. *Protein Sci.* **2000**, *9* (7), 1274−1281.
(65) Taggart, C.; Cervantes-Laurean, D.; Kim, G.; McElvaney, N. G.; Wehr, N.; Moss, J.; Levine, R. L. Oxidation of Either Methionine 351 or Methionine 358 in A1-Antitrypsin Causes Loss of Anti-Neutrophil Elastase Activity. *J. Biol. Chem.* **2000**, *275* (35), 27258−27265.
(66) Hawkins, P.; Sya, J.; Hup, N. K.; Murphy, M. P.; McElvaney, N. G.; Reeves, E. P. Alpha-1 Antitrypsin Augmentation Inhibits Proteolysis of Neutrophil Membrane Voltage-Gated Proton Channel-1 in Alpha-1 Deficient Individuals. *Medicina* **2021**, *57* (8), 814.
(67) Cruz, M. A.; Bohinc, D.; Andraska, E. A.; Alvikas, J.; Raghunathan, S.; Masters, N. A.; van Kleef, N. D.; Bane, K. L.; Hart, K.; Medrow, K.; Sun, M.; Liu, H.; Haldeman, S.; Banerjee, A.; Lessieur, E. M.; Hageman, K.; Gandhi, A.; de la Fuente, M.; Nieman, M. T.; Kern, T. S.; Maas, C.; de Maat, S.; Neeves, K. B.; Neal, M. D.; Sen Gupta, A.; Stavrou, E. X. Nanomedicine Platform for Targeting Activated

Neutrophils and Neutrophil−Platelet Complexes Using an A1-Antitrypsin-Derived Peptide Motif. *Nat. Nanotechnol.* **2022**, *17* (9), 1004−1014.
(68) Mendes, L. P.; Rostamizadeh, K.; Gollomp, K.; Myerson, J. W.; Marcos-Contreras, O. A.; Zamora, M.; Luther, E.; Brenner, J. S.; Filipczak, N.; Li, X.; Torchilin, V. P. Monoclonal antibody 2C5 specifically targets neutrophil extracellular traps. *PubMed* **2020**, DOI: 10.1080/19420862.2020.1850394.
(69) Skallberg, A.; Bunnfors, K.; Brommesson, C.; Uvdal, K. Neutrophils Activated by Nanoparticles and Formation of Neutrophil Extracellular Traps: Work Function Mapping and Element Specific Imaging. *Anal. Chem.* **2019**, *91* (21), 13514−13520.
(70) Kim, S.-J.; Kim, J.; Kim, B.; Lee, W.-W.; Liu, X.; Chang, Y.-T.; Park, J.-W. Validation of CDr15 as a New Dye for Detecting Neutrophil Extracellular Trap. *Biochem. Biophys. Res. Commun.* **2020**, *527* (3), 646−653.

https://doi.org/10.1021/acsami.4c20658
ACS Appl. Mater. Interfaces 2025, 17, 9140−9154